JOURNAL OF GEOPHYSICAL RESEARCH, VOL. 103, NO. C9, PAGES 18,405–18,423, AUGUST 15, 1998

# A climatology of the shelfbreak front in the Middle Atlantic Bight

Christopher A. Linder

Massachusetts Institute of Technology/Woods Hole Oceanographic Institution Joint Program in Oceanographic Engineering, Woods Hole, Massachusetts

Glen Gawarkiewicz

Woods Hole Oceanographic Institution, Woods Hole, Massachusetts

**Abstract.** Description of the shelfbreak front in the Middle Atlantic Bight is hampered by the extreme variability of the front. In order to gain insight into both the seasonal variability and regional variations in the mean frontal structure and associated baroclinic jet, historical data are used to produce two-dimensional climatological fields of temperature and salinity for the region south of Nantucket shoals, along the south flank of Georges Bank, and off the coast of New Jersey. Associated cross-shelf fields of density and geostrophic velocity are also computed. The climatological temperature and salinity are consistent with previous descriptions of the frontal hydrography. The temperature contrast across the front varies seasonally between 2° and 6°C. The salinity contrast is 1.5-2, with little seasonal variation. The near-surface density gradients are strongest during the winter and weakest during the summer, when the seasonal thermocline is established. The cross-frontal density gradients are strongest near the foot of the front. Despite the inherent smearing of frontal gradients incurred by averaging over large temporal and spatial scales, the geostrophic velocity field south of Nantucket shows a strong (0.2-0.3 m $s^{-1}$) baroclinic jet associated with the frontal density gradients. The core of the jet, having a width of 15-20 km, is located near the 150-m isobath. Transport calculations for the flow over the outer shelf and slope are in the range of 0.2-0.3 Sverdrups (Sv) to the west. This is comparable to the estimated transport (0.4 Sv) shoreward of the 100-m isobath.

## 1. Introduction

The shelfbreak front in the Middle Atlantic Bight is the water mass boundary between the cool, fresh water of the continental shelf and the warm, saline water of the continental slope. The front has been described in numerous studies dating back to *Bigelow* [1933] and is important in many of the commercial fisheries of the Middle Atlantic Bight because of the enhanced primary productivity associated with the front [*Marra et al.*, 1990].

In addition to the numerous theoretical studies of the front, observational studies of the front have fallen into three broad categories: intensive hydrographic surveys, typically with numerous cross-frontal transects; long-term mooring arrays with current meters and thermistors; and climatologies.

Each of these methods has its strengths and weaknesses in describing the front. Intensive hydrographic surveys, such as those by *Beardsley and Flagg* [1976] and *Burrage and Garvine* [1988], offer synoptic snapshots which generally resolve the thermohaline structure of the front but are subject to the limitation of the station spacing and the larger question of how representative such short-term observations actually are. Long-term mooring arrays, such as the Nantucket Shoals Flux Experiment (NSFE) [*Beardsley et al.*, 1985] and the Shelf Edge Exchange Processes experiments (SEEP I [*Aikman et al.*, 1988; *Houghton et al.*, 1988]; and SEEP II [*Houghton et al.*, 1994; *Flagg et al.*]), 1994, address the longer-term statistics of the velocity and temperature structure of the front but have been limited by the horizontal and vertical scales which have been resolved.

Climatologies are useful in describing the "mean" frontal conditions. Several studies have examined the front and its motions in terms of climatologies. The most comprehensive study to date is that of *Wright* [1976], who examined primarily temperature data to define the mean frontal position and its seasonal variations. Using the 10°C isotherm as a criterion for the position of he front, he found that the surface outcrop of the front varied seasonally, extending much farther



Paper number 98JC01438
0148-0227/98/98JC-01438$09.00

offshore during the summer than in the winter. He also found that the surface outcrop of the front was much more variable than the position of the foot of the front, which was generally within 10 km of the 100-m isobath. *Halliwell and Mooers* [1979], using surface thermal imagery, described the mean position and variability of the surface thermal front.

More recently, *Naimie et al.* [1994] used a three-dimensional climatology of the density field along with the tidal residual flow field over Georges Bank and the Gulf of Maine to produce bimonthly averaged flow fields. They found that near the shelfbreak, a jet with typical maximum velocities of 0.2–0.25 m $s^{-1}$ was present. Their domain, however, only extended seaward to the 200-m isobath.

In order to compensate for the scarcity of data, we have used a method similar to *Pickart* [1992] for collapsing widely scattered three-dimensional data into an "average" two-dimensional section. Fields of temperature, salinity, density, and alongshelf geostrophic velocity for the outer shelf and upper slope in the Middle Atlantic Bight are computed. Fields of relative and potential vorticity are then computed from the velocity and density fields. Our primary motivation to perform this study has been to contrast climatological fields with recent shipboard measurements of the front in which the frontal jet has velocities as large as 0.5 m $s^{-1}$ and widths as small as 10 km [*Gawarkiewicz et al.*, 1996]. Thus we will concentrate on establishing the seasonal variation in the climatological velocity structure as well as the potential vorticity distribution of the jet.

The outline of this paper is as follows. In section 2, the historical data and the methods for averaging are described. The thermohaline and density fields are presented in section 3, while the seasonal progression of the front appears in section 4. The geostrophic velocity fields and jet structure are described in section 5, and the relative and potential vorticity fields are described in section 6. The results are discussed in section 7, and the conclusions are presented in section 8.

## 2. Methods

The focus of this climatological study is the New England continental shelf south of Nantucket Shoals (39°-41°N, 69°-72° W, hereinafter referred to as NS). The region is convenient for a climatological study because there are few major bathymetric features, the station density is relatively high, and it encompasses almost a quarter of the area of the Middle Atlantic Bight (MAB) [*Wright*, 1976]. To illustrate interregional comparisons, climatological mean fields have also been computed for the south flank of Georges Bank (GB)(39.5°-41.5° N, 65.5°-68.5° W), and a section of the MAB east of New Jersey (NJ)(37-39.5° N, 72.5°-75.5° W). These regions and selected isobaths are shown in Figure 1.

*Curry*'s [1996] HydroBase database is the data source for this climatology. HydroBase is a database of hydrographic profiles obtained from the National Oceanographic Data Center (NODC) collected from the early 1900s to April 1990. Deep-water stations (200 m or greater water depth) were subjected to a vigorous quality control process in which realizations with temperature and salinity characteristics more than 2.3 standard deviations away from the mean were discarded [*Curry*, 1996]. The extreme variability of coastal hydrography precluded quality control based on standard deviations in shallow (<200 m depth) regions.

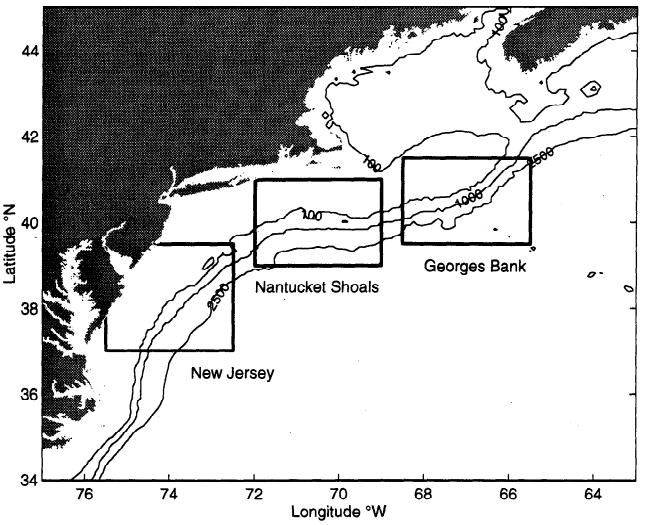


**Figure 1.** The bathymetry and chosen study areas for averaging hydrographic data within the Middle Atlantic Bight. The primary region of interest is Nantucket Shoals (NS), along with Georges Bank (GB) and New Jersey (NJ).

Figure 2 shows the histogram of HydroBase stations in the NS region plotted by year. A total of 3240 stations were extracted for NS. This is more than double the hydrographic stations used in the [*Wright* 1976] climatology, although he also included 19,000 bathythermograms measuring only temperature. Generally, more stations were occupied during the summer (820 for the NS August-September time period versus 432 for December-January). The station distributions for GB and NJ are both similar seasonally to NS, although smaller in magnitude (2150 total stations for GB and 2765 for NJ).

For the small scales and shallow water of the region of interest here, both three-dimensional isopycnal averaging [*Curry*, 1996; *Lozier et al.*, 1994] and three-dimensional spatial averaging were insufficient for creating a statistically significant mean field. Instead, a depth bin averaging method was implemented to maximize the number of contributions to the mean and to minimize averaging water masses with different properties. A similar method was used by *Pickart* [1992] to compare 12 hydrographic sections through the Gulf Stream. *Pickart* [1992] converted each of the sections to a height above bottom versus bottom depth coordinate system to allow for comparison of sections from differ-

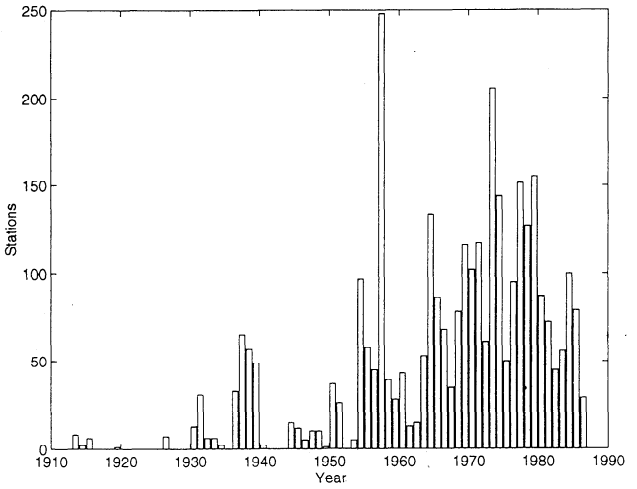


**Figure 2.** The yearly distribution of hydrographic stations used for producing the NS fields.

ent hydrographic regions. He then regridded each of the sections onto a regular grid, facilitating easy comparison of the sections from each region. Finally, he computed a mean field by averaging the 12 gridded sections.

Depth bin averaging, using a simple procedure, creates a single two-dimensional cross-shelf transect of properties based on hydrocasts from a three-dimensional ocean volume. First, the NODC data were extracted in bimonthly groups from HydroBase for the study region [*Curry*, 1996]. Next, an average bathymetric profile aligned perpendicular to the local isobaths was computed for the region based on ETOPO5 bathymetry data. Then, a set of depth bins in which to segregate the casts was selected. The number and size of the bins were chosen based on the total number of casts per bin and the cross-shelf spacing of the bins. This resulted in a small number of widely spaced bins over the shelf and a concentration of bins near the shelfbreak. This selection allowed for peak cross-shelf resolution near the shelfbreak, where the strongest gradients typically occur. After selecting the bins, the data were sorted into the bins based on their echo sounder depth values. Casts without echo sounder depths (roughly 16% for NS) were discarded. Then, the data were segregated further into vertical bins, 10 m over the shelf and 50 m in the deep slope waters. An arithmetic mean of each vertical bin was then computed. Finally, the mean data were transformed to a cross-shelf distance versus depth profile by assigning a cross-shelf distance to each depth bin. The cross-shelf distances in this climatology were found by linearly interpolating the average bathymetric profile and are all measured in km from the 100-m isobath, with positive distance denoting the offshore direction. Figure 3 shows the location of the averaged points for NS, clearly illustrating the concentration of bins near the shelfbreak (four cross-shelf grid points within 20 km). Figure 4 shows the cross-shelf distribution of stations for each seasonal period and echo sounder depth bin, revealing the high number of stations in the shelfbreak bins. The station density is relatively constant seasonally and spatially, although sampling increased slightly during the summer months. The depth bin method allows a large number of data points to be included (across three degrees of longitude for NS).

There is a potential bias using this method if stations within a depth bin are systematically located at one edge of the bin. Therefore, at an early stage of the processing, the spatial distribution of the stations was examined to determine whether or not the distribution of stations was affected by repeated sampling at specific positions or along particular isobaths. The station positions were not clustered or otherwise distributed in a manner to suggest that such biases were present within the data set.

The geostrophic velocity calculations presented here have been computed from statically stable density fields. The fields were calculated using the UNESCO 1983 polynomial [*Fofonoff and Millard*, 1983]. In the cases where hydrostatic instabilities existed in the raw density, the two vertical data points were replaced by the mean of the two points, weighted by the volume of the vertical bin. Multiple iterations were performed until the fields achieved stability. Usually no more than two iterations were required.

The geostrophic velocities were computed by integrating the thermal wind relation upward from a level of no motion at the bottom. A near-bottom current was used instead of the default zero-bottom velocity for the winter (February-March) and summer (August-September) NS fields. Figure 5 shows the averaged near-bottom current meter values taken from the NSFE experiment for summer and winter [*Beardsley et al.*, 1985]. It is important to note that the barotropic current is only significant over the shelf and is relatively weak near the shelfbreak. In all comparisons between

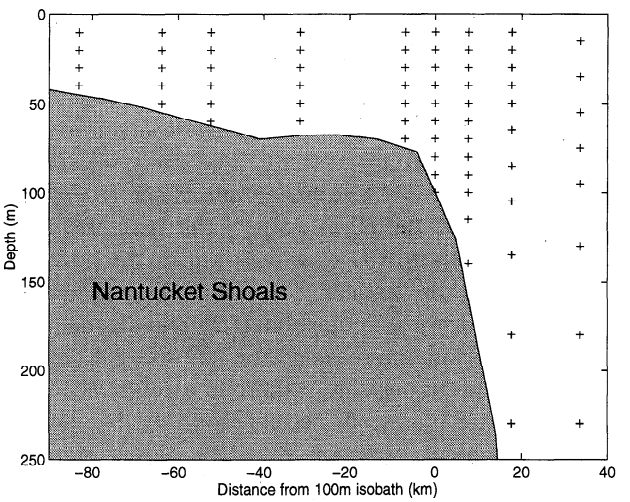


**Figure 3.** An averaged cross-shelf section (i.e., averaged bathymetric profile) showing the locations of the raw output grid points for the NS region.

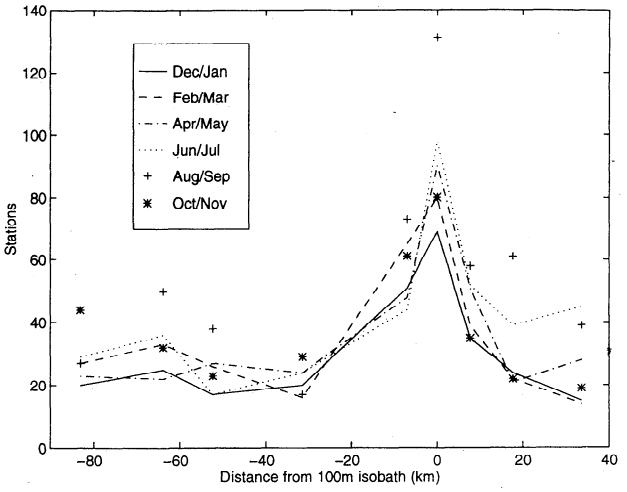


**Figure 4.** The cross-shelf and seasonal distribution of hydrographic stations used within the NS region.

the bimonthly time periods, a zero velocity was used at the bottom for all time periods.

## 3. Nantucket Shoals Thermohaline and Density Fields

We will now present the thermohaline and density fields for the NS region and compare them with the *Wright* [1976] climatology and some of the synoptic studies which have appeared previously. The temperature, salinity, and density fields by bimonthly period appear in Figures 6a, 6b, and 6c. Bold contours indicate the nominal frontal boundary chosen in previous works: the 10°C isotherm [*Wright*, 1976], the 34.5 isohaline [*Beardsley and Flagg*, 1976], and the $\sigma_t$=26.5 kg $m^{-3}$ isopycnal.

The temperature fields exhibit the greatest seasonal variability because the shallow shelf waters are strongly affected by the seasonal cycle of insolation. During the winter months, the temperature over the shelf becomes nearly homogeneous, presumably due to enhanced vertical mixing caused by storm activity and convective overturning at the surface [*Beardsley and Flagg*, 1976]. Figure 6a shows that this homogenization is most complete during February-March. The shelf waters vary between 4° and 6°C. *Beardsley and Flagg* [1976] show that seaward of the 80-m isobath the temperature increased more than 5°C over 5-25 km in the horizontal and 5-30 m in the vertical. The climatological temperature front is also particularly narrow and strong during this time period, increasing from 6° to 12°C over 20 km. Over the upper slope, there is a relatively homogeneous water mass outlined in Figure 6a by the 12°C isotherm, which corresponds to the "upper slope water pycnostad" defined by *Wright and Parker* [1976]. This feature is clearly evident in every time period except October-November. It appears most clearly during February-March, where it is slightly thicker (150 m) and is centered slightly deeper (150 m) than *Wright and Parker's* [1976] observations.

The April-May fields show the initiation of surface stratification, associated with decreasing storm activity and increasing insolation. The frontal boundary defined by the 10°C isotherm now intersects the surface about 10 km seaward of the shelf break. A stratified layer, approximately 25 m deep, has formed over the winter remnant of shelf water, also known as the "cold pool" [*Beardsley and Flagg*, 1976; *Houghton et al.*, 1982]. During June-July, the cold pool, defined by the 10°C isotherm, extends over the shelf and terminates close to the 90-m isobath, near the shelfbreak. As summer progresses (August-September), the thermocline deepens to almost 40 m. By August-September the areal extent of water with temperatures less than 10°C has significantly decreased in size. The cold pool is only about 20 m thick over the shelf and extends only to about the 80-m isobath in the cross-shelf direction. Convective overturning in late fall (October-November) acts to return the shelf to a homogenized state.

Figure 6b shows the seasonal evolution of the NS salinity structure. The qualitative salinity field characteristics remain relatively constant throughout the year despite variations in the local seasonal freshwater input cycle [*Bue*, 1970]. *Beardsley and Flagg* [1976] have observed that the salinity front, centered on the 34.5 isohaline, coincides with the temperature front during the winter. Figures 6a and 6b confirm this, especially during February-March. They also found that the salinity difference across the front was roughly 1-2 over 10-40 km in the horizontal and 20-35 m in the vertical. The climatological salinity gradient is comparable: roughly 1 over 20 km in the horizontal and 40 m in the vertical. Over the upper slope in the region of the upper slope pycnostad, the salinities are as high as 35.5 for many of

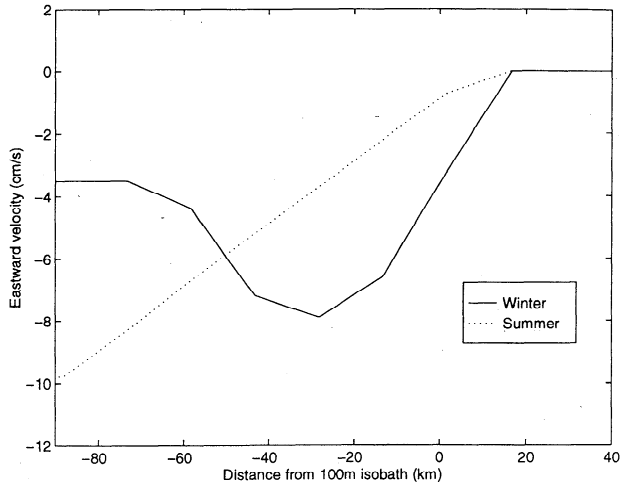


**Figure 5.** The cross-shelf distribution of seasonally averaged near-bottom velocities near Nantucket Shoals from the Nantucket Shoals Flux Experiment (NSFE) [*Beardsley et al.*, 1985].

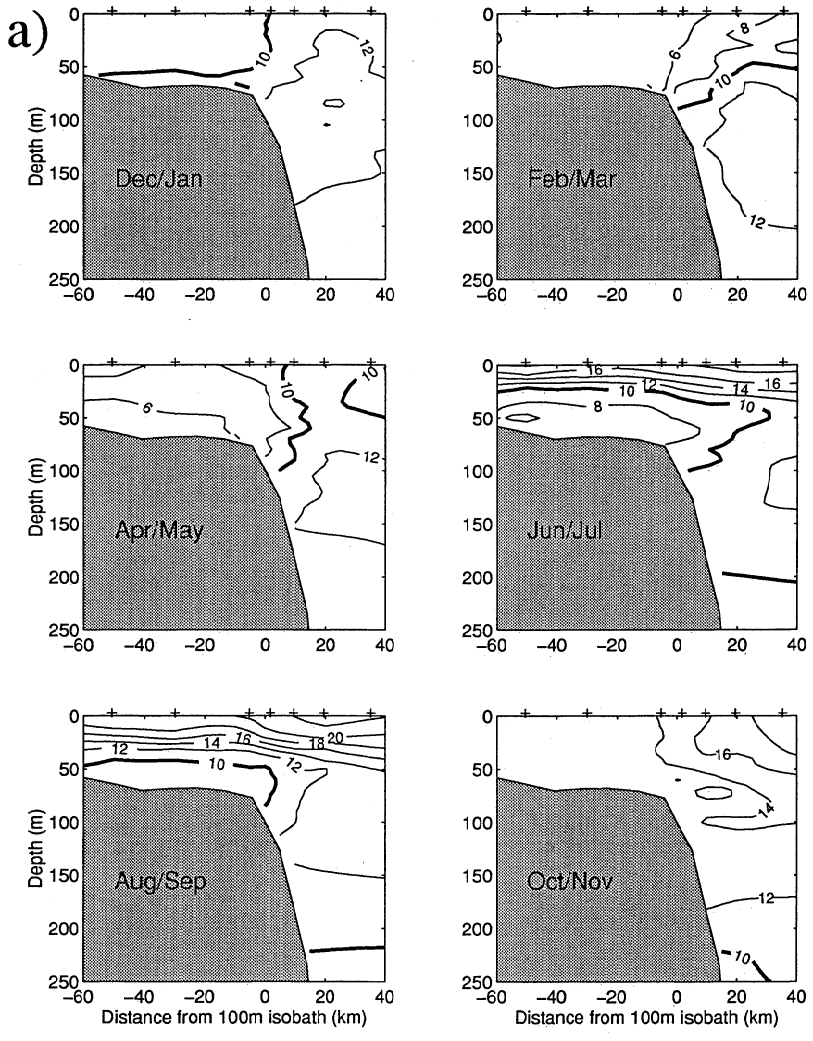


**Figure 6.** The bimonthly averaged fields for the NS region for (a) temperature, (b) salinity, and (c) density. The contour intervals are 2°C (Figure 6a),0.5 (Figure 6b), and 0.5 kg $m^{-3}$ (Figure 6c).

the time periods, which probably reflects the presence of warm core ring water mixing with the slope water.

The density fields are shown in Figure 6c. Since the salinity fields change little seasonally, the seasonal variations in the density field tend to be similar to the variability of the temperature fields. *Beardsley et al.* [1985] observed that during the winter months the density front has a well-defined surface outcrop and foot (bottom intersection) due to the homogeneity of the water masses. This is reflected in the December-January climatological density field and is somewhat evident in February-March. The low winter temperatures create a dense shelf water mass with densities greater than $\sigma_t$=26.0 kg $m^{-3}$. However, the high salinity of the slope waters leads to slope water densities greater than $\sigma_t$=26.5 kg $m^{-3}$.

The development of the seasonal pycnocline is evident as early as April-May, when surface densities decrease below $\sigma_t$=26 kg $m^{-3}$. By June-July, the upper pycnocline is fully developed, with a vertical density difference of over 2 kg $m^{-3}$ over 25 m ($N^2 = 0.76 \times 10^{-3}$ $s^{-2}$). In the upper pycnocline, the slope of the front, defined by the $\sigma_t$=26.5 isopycnal, has decreased significantly. Now a common density surface connects the shelf and slope waters, as *Aikman*[1984] has shown. The August-September period shows a "typical" summer density field. The vertical stratification in the surface pycnocline has now strengthened to a vertical density difference of 3 kg $m^{-3}$ ($N^2 = 1.1 \times 10^{-3}$ $s^{-2}$), which is within the range of 3.0-4.0 kg $m^{-3}$ observed by *Beardsley and Flagg* [1976]. Increased storm activity and convective cooling weaken the pycnocline during autumn(October-November), giving a similar structure to that computed for the spring months (April-May). It is important to note that although the upper level thermocline causes the near surface isopycnals in the frontal region to flatten, they retain a positive slope near the shelfbreak throughout the year beneath the seasonal pycnocline and are particularly strong near the foot of the front.

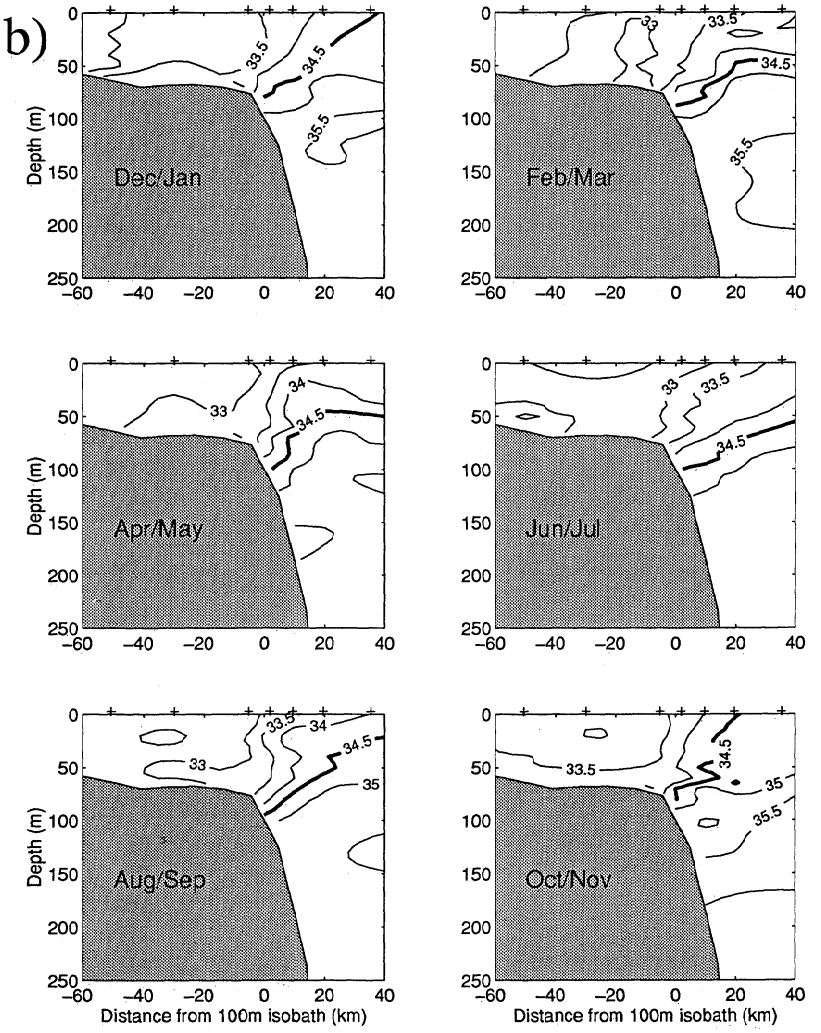


**Figure 6. (continued)**

The cross-shelf density contrast is useful in quantifying the strength of the front and the associated baroclinic current shear. *Beardsley and Flagg* (1976) found that for March 1974, the average cross-frontal density contrast was 0.5 kg $m^{-3}$. They did not specify the horizontal or vertical intervals over which the densities were averaged. To better quantify this cross-shelf density difference, the onshore density (averaged over a 10-km interval from 30 to 20 km shoreward of the 100-m isobath) has been subtracted from the offshore density (averaged over a 10-km horizontal interval from 20 to 30 km seaward of the 100-m isobath) using the regularly gridded field. This has been repeated for three different depth intervals (5-15 m, 25-35 m, and 45-55 m), to illustrate the depth dependence. Figure 7 shows the results of these calculations for the NS subset, plotted as a function of time. During December-January, the density difference is approximately 0.3 kg $m^{-3}$ and is nearly independent of depth, reflecting the lack of vertical stratification over the shelf and slope. During February-March, the surface density contrast drops to 0.23 kg $m^{-3}$, while the deep (45-55 m) density contrast increases to 0.47 kg $m^{-3}$. As the spring progresses into summer, the density contrasts diverge further with depth. The maximum range in temperature contrast occurs in August-September, corresponding to the period of most intense stratification. During this time period, the extremes in density contrast are approximately 0 kg $m^{-3}$ in the surface waters (5-15 m) and 0.5 kg $m^{-3}$ beneath the seasonal pycnocline (45-55 m). The extremely low density contrast in the surface waters is primary due to surface heating [*Aikman*, 1984], using a one-dimensional, two-layer bulk-mixing model). By October-November the density contrast becomes more uniform with depth.

The density gradients near the foot of the front are particularly important for the thermal wind shear. The typical density gradients near the foot of the front are 0.2 kg $m^{-3}$ over 10 km, which gives a value of $M^2 = (g)/(\rho_0)\ (\partial\rho)/(\partial x)$=1.9 $\times 10^{-7} s^{-2}$ or $M = 4.4 \times 10^{-4} s^{-1}$. This remains relatively constant throughout the bimonthly time periods, although the cross-shelf position of the foot of the front varies throughout the time periods.

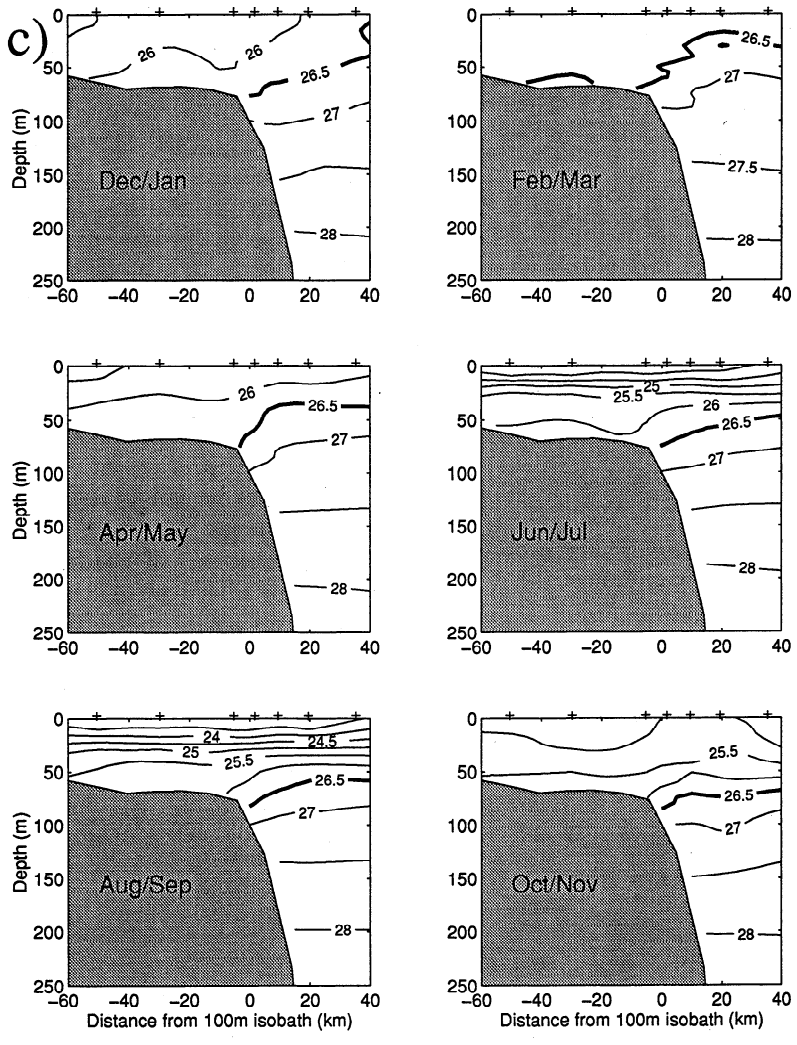


**Figure 6. (continued)**

The standard deviations of the temperature fields for the winter (February-March) and summer (August-September) time periods appear in Figure 8. The largest values of the standard deviations occur within the frontal zone. (Note that in addition to the inherent physical variability, these standard deviations also include possible contributions from sampling bias and data sparseness.) During the winter, the standard deviation is less than 1.5°C shoreward of the frontal zone and over the continental slope beneath the frontal zone. However, within the frontal zone this is as large as 2.5°C. The maximum values are over 3.5°C near the surface over the upper slope. During the summer, the largest standard deviations are roughly 4.5°C and are located near the seasonal thermocline at the offshore edge of the cold pool. This is the position where *Houghton et al.* [1988] measured the largest cross-shelf heat fluxes from the SEEP I mooring array and where *Garvine et al.* [1989] measured the largest cross-shelf heat fluxes from a series of synoptic hydrographic surveys during the summer. This is also the position of maximum isopycnal motion for the summer case of the linearized stability analysis performed by *Gawarkiewicz* [1991] corresponding to the pycnocline-trapped mode.

The spatial structure of the standard deviations of salinity in winter (Figure 8c) is similar to that of temperature, with larger values in the vicinity of the front as well as near the surface over the continental slope. Values within the front are 0.6, double those on the shelf and over the slope beneath the front. Near the surface over the slope, the standard deviation is as large as 1.5. The spatial structure of the salinity variability in summer differs from that of temperature (Figure 8d). The maximum value of 1.3 occurs over the slope near the surface and decreases moving both shoreward near the surface and beneath the maximum. There is no mid-depth maximum as in the temperature field.

The effects of these temperature and salinity changes on the density field are shown in Figure 9 for both temperature and salinity separately. The standard deviation of density was obtained by adding to the mean field either temperature or salinity of 1 standard deviation and holding the other property fixed. The density field was then computed using the equation of state. Then

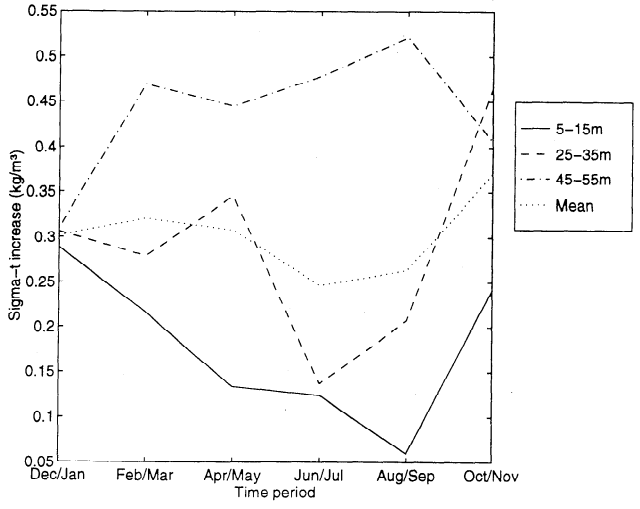


**Figure 7.** The seasonal variation of the cross-shelf density difference for NS at various depths.

the density value from the original mean field was subtracted to give the standard deviation of the density.

During winter, the temperature variations result in density standard deviations of 0.3-0.4 kg $m^{-3}$ in the frontal zone, with values as large as 0.5 kg $m^{-3}$ near the surface over the slope (Figure 9a) 0.9 kg $m^{-3}$, in the vicinity of the seasonal thermocline near the offshore edge of the cold pool. The values in other areas are largest in the vicinity of the seasonal thermocline (depths of 10-30 m), with values of 0.5-0.7 kg $m^{-3}$. Density standard deviations due to salinity during the winter (Figure 9c) are 0.4-0.6 kg $m^{-3}$ within the frontal zone and up to 1.0 kg $m^{-3}$ near the surface over the continental slope. Maximum summer values of the standard deviation of density due to the salinity variations (Figure 9d) are 0.9 kg $m^{-3}$ on the surface over the continental slope.

A comparison of the frontal structure from the climatology with typical synoptic sections (that is unperturbed by warm-core rings or large frontal instabilities)

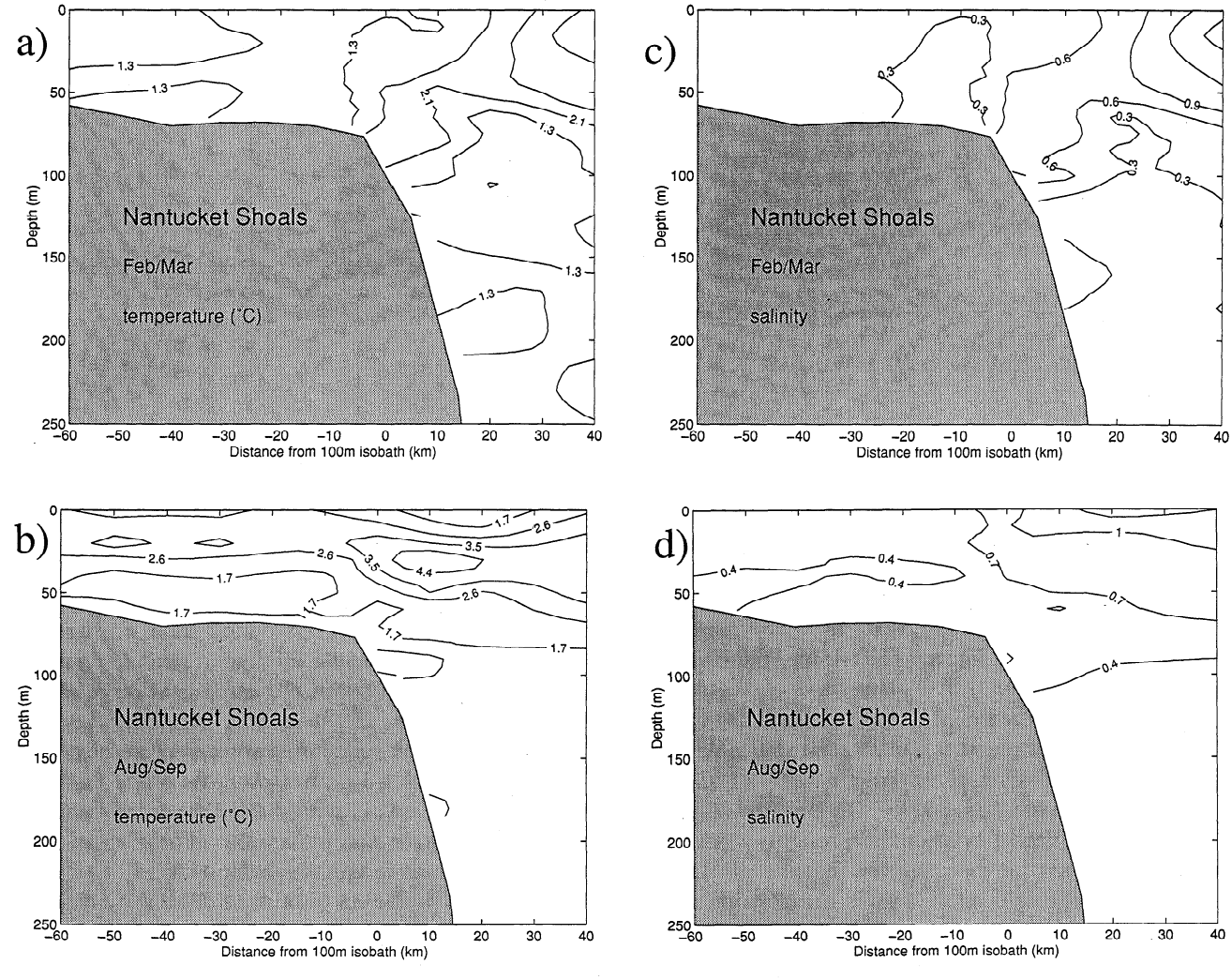


**Figure 8.** Variability of the temperature and salinity fields from the NS region. (a) Temperature standard deviations during winter (February-March). (b) Temperature standard deviations during summer (August-September). (c) Salinity standard deviations during winter (February-March). (d) Salinity standard deviations during summer (August-September).

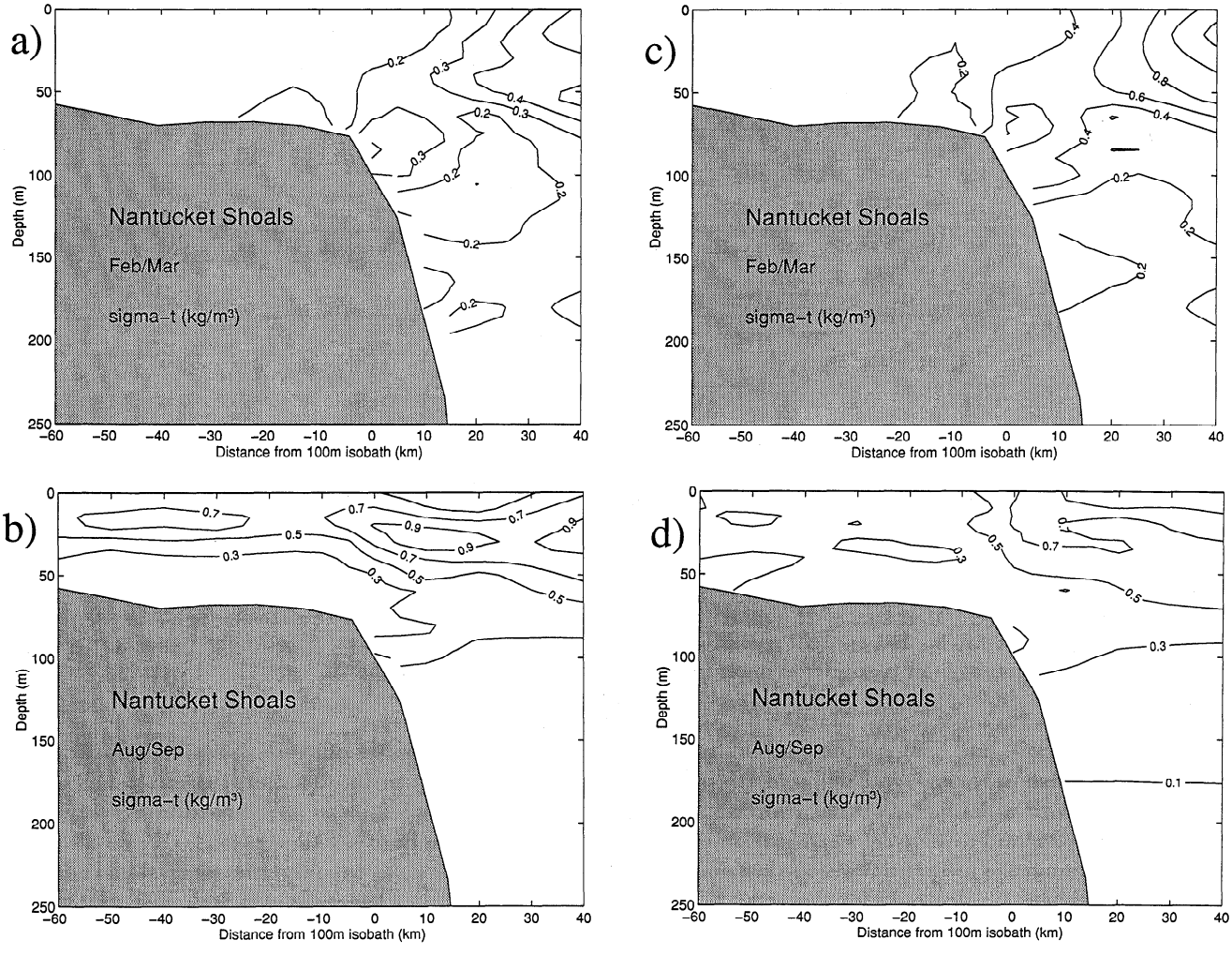


**Figure 9.** Variability of the density field in the NS region. (a) Density standard deviations based on temperature during winter. (b) Density standard deviations based on temperature during summer. (c) Density variations based on salinity during winter. (d) Density variations based on salinity during summer.

shows a relatively good agreement. Figure 10 shows the climatology in February-March from a depth of 5-15 m (upper panels) and 45-55 m (lower panels) as well as a winter section taken from the SEEP-I program [*Houghton et al.*, 1988]. (The error bars in Figure 10 indicate plus and minus one standard deviation of the climatological temperature and salinity fields.) The surface values of the climatology do not extend offshore far enough to reach typical slope values of 12°C and 35.0 salinity but show cross-shelf values of temperature and salinity which are comparable in magnitude, although displaced slightly in cross-shelf position. The salinities from the synoptic section are lower than the climatology, which may be due to the large interannual salinity variations [e.g., *Manning*, 1991]. At middepth (lower panels), the curves are very similar, with the salinity values again being slightly lower than the climatology. Comparisons for the summer (Figure 11) show even better similarity in cross-shelf structure between the climatology and a synoptic section from SEEP I at both the surface and middepth.

Thus, as anticipated, the thermohaline fields evolve seasonally in a manner consistent with previous descriptions of the shelf and slope. Let us now concentrate on the seasonal evolution of the frontal position.

## 4. Seasonal Progression

We will now present the evolution of the shelfbreak front as it is defined by the 34.5 isohaline. The mean position and seasonal progression of the shelfbreak front have been studied using advanced very high resolution radiometer (AVHRR) satellite measurements of the sea surface temperature (SST) [*Halliwell and Mooers*, 1979; *Drinkwater et al.*, 1994] and on mean fields of the hydrography [*Wright*, 1976; *Flagg et al.*, 1982]. A summary of mean frontal position and slope estimates is given in Table 1 for selected authors.

The bimonthly position of the NS 34.5 isohaline is shown in Figure 12a. The isohaline intersects the bottom between the 85- and 105-m isobaths throughout the year. This range of isobaths corresponds to a cross-shelf

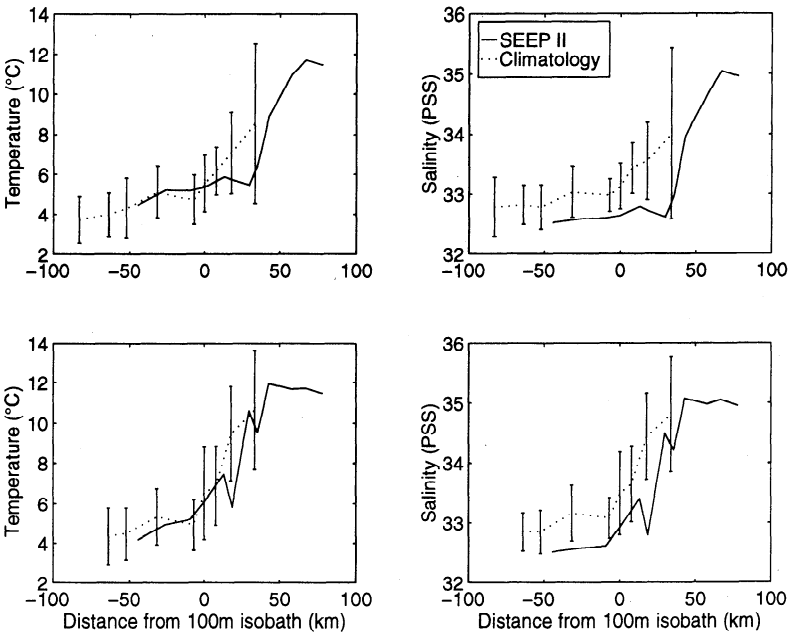


**Figure 10.** Comparison of the climatology (dotted lines) and a synoptic section (solid lines) from the Shelf Edge Exchange Processes (SEEP I) program during winter. The upper panels are from a depth of 5-15 m, and the lower panels are from a depth of 45-55 m.

distance of about 10 km. The isohaline generally slopes upward and offshore from the shelfbreak throughout the year but with a distinct seasonal transition. During October-November, when the stratification over the shelf is weakening, the mean frontal slope is a maximum and intersects the surface only 20 km away from the bottom outcrop (giving a slope of roughly $5 \times 10^{-3}$). However, this slope decreases to roughly half ($2\text{-}3 \times 10^{-3}$) during December-January, as the surface position of the front moves offshore. The 34.5 isohaline does not intersect the surface (within the cross-shelf extent of the climatology, out to 40 km seaward of the shelfbreak) during any other time period. While all of the 34.5 isohalines have roughly the same slope near the bottom outcrop of the front, the isohaline flattens out during the other time periods in the upper portion of the water column. Thus the front may be characterized by two frontal slopes: a relatively constant slope in the

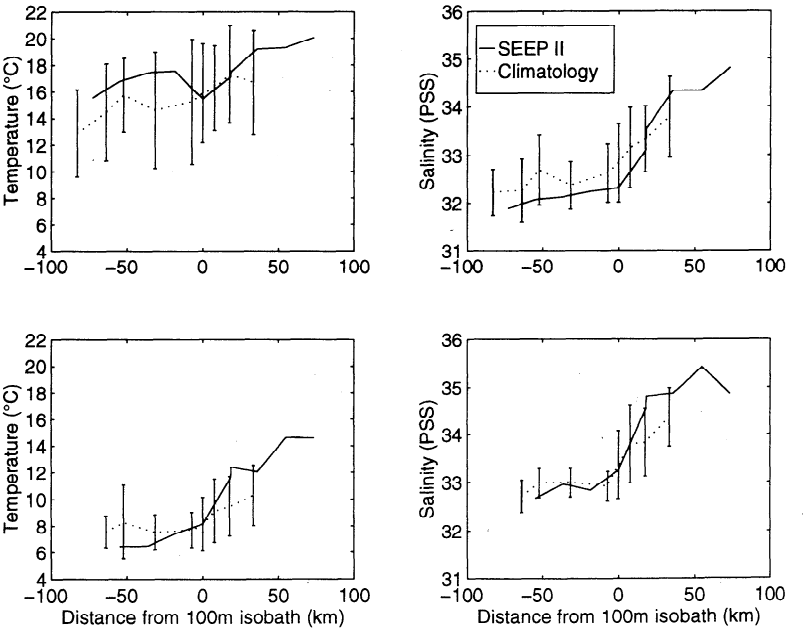


**Figure 11.** Comparison of the climatology (dotted lines) and a synoptic section (solid lines) from the SEEP I program during summer. The upper panels are from a depth of 5-15 m, and the lower panels are from a depth of 45-55 m.

**Table 1.** Recent Examples of Frontal Outcrop and Slope Measurements

| Reference | Region/ Season | Method | Surface (s) Bottom (b) Frontal Position | Mean Frontal Slope | Miscellaneous |
|---|---|---|---|---|---|
| *Beardsley and Flagg* [1976] | New England shelf, winter | field experiment | 80-m isobath (b) | $2x10^{-3}$ | westward currents observed over shelf |
| *Voorhis et al.* [1976] | New England shelf, late spring | field experiment | 100-m isobath (b) | not given | 0.7 Sv transport in baroclinic jet |
| *Wright* [1976] | New England shelf, all seasons | climatological 1941-1972 | 100-m isobath (b) | not given | analyzed mostly thermograms |
| *Halliwell and Mooers* [1979] | Entire Middle Atlantic Bight all seasons | climatological, based on satellite sea surface temperature | 80 km seaward of shelfbreaks (s) | not given | based on surface temperature |
| *Flagg et al.* [1982] | Georges Bank, all seasons | climatological 1975-1979 | 100-m isobath (b) | $2.8 \times 10^{-3}$ | 2 km/month summer frontal migration |
| *Burrage and Garvine* [1988] | New Jersey shelf, summer | synthesis of 12 transects | $\sim$ 80-m isobath (estimated from plot) | not given | computed standard deviation of T structure |
| *Houghton et al.* [1988] | New England shelf, full year | field experiment | 100-m isobath (b) | $2.2 \times 10^{-3}$ (winter) $1.3 \times 10^{-3}$ (summer) | focused on cross-shelf exchange |
| *Drinkwater et al.* [1994] | Entire Middle Atlantic Bight all seasons | climatological, based on satellite sea surface temperature 1972-1994 | $\sim$ 40 km seaward of shelfbreak at 70°W (s) | not given | also found $\pm$ 20-km interannual deviation |

lower half of the water column and a seasonally variable slope in the upper half of the water column. We refer to this break in the slope of the frontal isohalines as the inflection point of the front.

Although the slope of the front near the shelfbreak remains relatively constant, the mean position of the frontal bottom outcrop exhibits a slight seasonal migration. During October-November and December-January the front is at its extreme onshore position. The front reaches its maximum offshore position in June-July. The August-September bottom outcrop is displaced significantly shoreward (3-4 km horizontally or 10-15 m vertically). This onshore retreat continues through the winter, when the front reaches its most shoreward position. This is consistent with both the previous observation of freshest shelf water during June-July (Figure 6b) and *Manning's* [1991] observations from the National Marine Fisheries Service's (NMFS) Marine Resources, Monitoring, And Prediction (MARMAP) hydrographic surveys. Manning showed that during the summer, the isohalines exhibit a change in slope at middepth (20-40 m), qualitatively matching the NS climatological data shown in Figures 6b and 12a.

Some contradictions can be found between this climatology and *Wright's* [1976] conclusions. Wright estimated the mean position of the foot of the front to be at its extreme offshore location during the winter. *Wright's* [1976] plot of the surface expression agrees well with the climatology, showing the front at its maximum offshore position during July and its minimum onshore position during the winter.

This analysis has been repeated for GB and NJ. The GB isohalines, shown in Figure 12b, differ from the NS positions. The GB isohalines in the region near the shelfbreak in the lower portion of the water column have a smaller slope than NS (roughly $2 \times 10^{-3}$), and no isohalines physically intersect the surface within the domain at any time of the year. The inflection point between the isohaline slopes occurs higher in the water column (between 40 and 50 m). The foot of the front occurs at a minimum depth of 110 m from October-November through December-January. The maximum

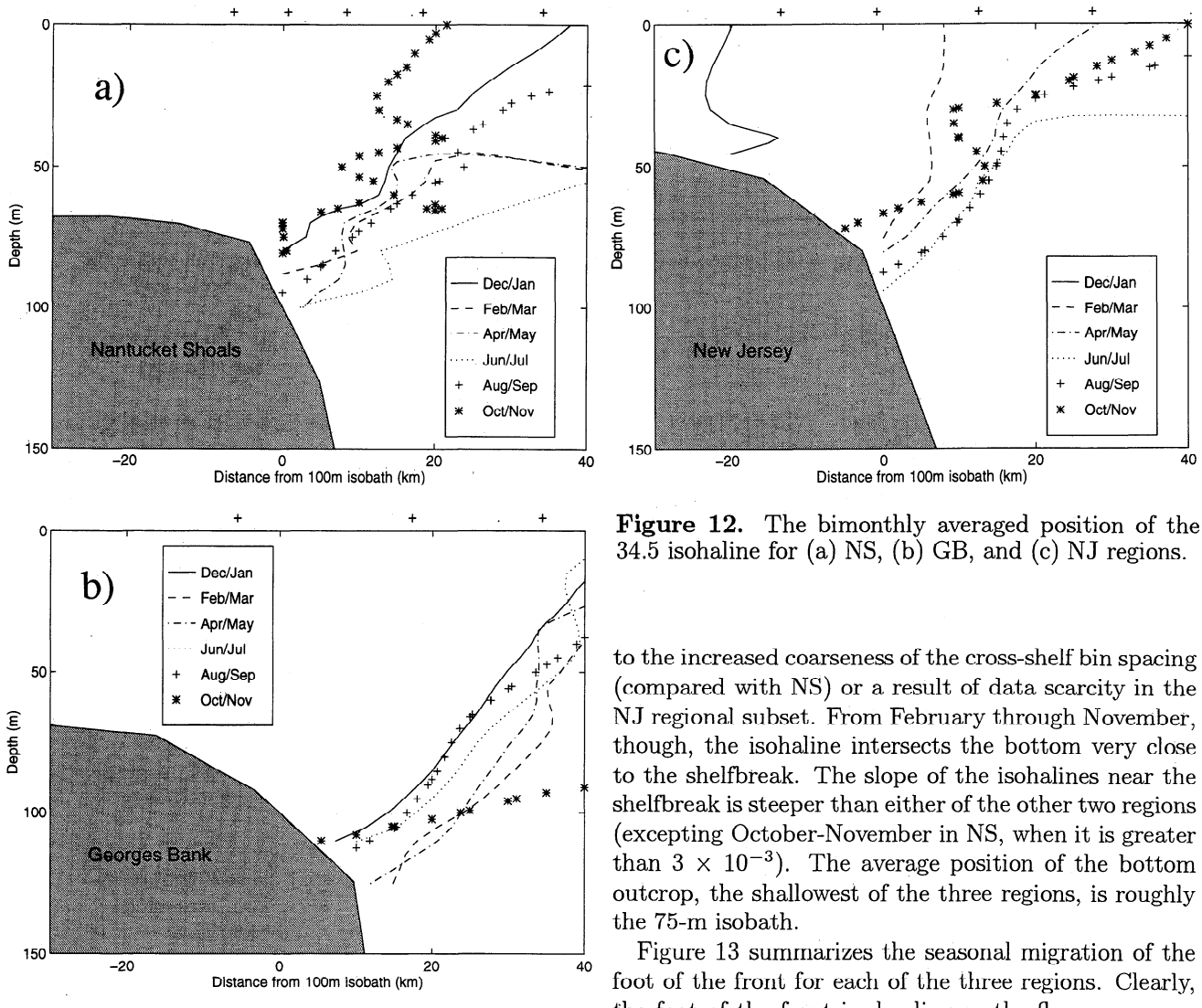


**Figure 12.** The bimonthly averaged position of the 34.5 isohaline for (a) NS, (b) GB, and (c) NJ regions.

depth of the foot, at about 130 m depth, occurs during February-March and April-May. During the summer months the front moves onshore to roughly the 110 m isobath again. *Flagg et al.* [1982] also showed an onshore frontal migration during the summer. However, the climatology shows an offshore adjustment during the winter (February-March), while *Flagg et al.* [1982] observed this movement in late fall. The seasonal cycle is much less clearly defined compared with NS, and the average position of the foot of the front, at the 120-m isobath, is deeper, most likely corresponding to the deeper average shelfbreak depth in this region. *Manning's* [1991] Great South Channel mean salinity profiles show a slightly shallower frontal bottom outcrop (roughly the 100-m isobath). They also show very little seasonal variability, as is shown for GB in Figure 12b.

In contrast to both GB and NS, the NJ isohalines, shown in Figure 12c, exhibit a surface expression for this given cross-shelf range in every time period except June-July and August-September. The December-January curve is anomalous because it is almost 20 km shoreward of every other bimonthly curve. This may be due to the increased coarseness of the cross-shelf bin spacing (compared with NS) or a result of data scarcity in the NJ regional subset. From February through November, though, the isohaline intersects the bottom very close to the shelfbreak. The slope of the isohalines near the shelfbreak is steeper than either of the other two regions (excepting October-November in NS, when it is greater than $3 \times 10^{-3}$). The average position of the bottom outcrop, the shallowest of the three regions, is roughly the 75-m isobath.

Figure 13 summarizes the seasonal migration of the foot of the front for each of the three regions. Clearly, the foot of the front is shoaling as the flow progresses to the southwest. It is important to note that although the annual mean position of the bottom outcrop varies substantially by region, the bathymetry also changes substantially. The overriding trend is for the shelfbreak front, marked by the 34.5 isohaline, to manifest itself on or near the shelfbreak (Table 2). *Wang* [1984], *Chapman* [1986], *Gawarkiewicz and Chapman* [1992], and *Condie* [1993] have also studied this characteristic through different models using different assumptions.

Figure 13 also reveals a spatial lag in the frontal migration. This is most readily apparent when considering the time period of extreme offshore frontal position (the deepest foot of the front). The front is at its maximum offshore position during February-March for GB, April-May or June-July for NS, and June-July for NJ. Despite the coarse temporal scale of the study, it is tempting to consider a seasonal freshwater pulse traveling southward through the MAB, displacing the frontal boundary seaward. This would imply an alongshelf advection rate of roughly 0.08 m $s^{-1}$. This would be consistent with *Chapman et al.* [1986] and *Chapman and Beardsley* [1989] circulation schemes, which show the continuity of the shelf flow from the Scotian Shelf through the

**Table 2.** Frontal Jet Characteristics (Annual Average)

| Region | Shelfbreak Depth m, | Foot of Front, m | Isobath With Maximum Jet Velocity, m | Vertical Scale of Jet, m | Jet Width, km | Jet Transport, Sv | Maximum Jet Velocity, m $s^{-1}$ |
|---|---|---|---|---|---|---|---|
| Georges Bank | 125 | 120 | 275 | 75 | 47 | 0.45 | 0.16 |
| Nantucket Shoals | 100 | 95 | 145 | 62 | 21 | 0.24 | 0.22 |
| New Jersey | 75 | 75 | 162 | 56 | 19 | 0.16 | 0.15 |

Gulf of Maine and the Middle Atlantic Bight. However, *Mountain* [1991] has shown that the variability in the interannual signal of the freshwater content of the shelf is at least as strong as the seasonal signal, and so it is difficult to establish the seasonal cycle of the freshwater content.

## 5. Geostrophic Velocity Structure and Associated Transports

Using the density field described in section 2, we will now use the thermal wind relation to calculate the geostrophic velocity field associated with the front. The thermal wind relation is

$$v_z = \frac{-g}{\rho_0 f}\frac{\partial \rho}{\partial x} \tag{1}$$

where $v$ is the along-isobath velocity, $g$ is the gravitational acceleration, $\rho_0$=1026 kg $m^{-3}$ is the mean density, $f$ is the Coriolis parameter ($10^{-4}$ $s^{-1}$), and the subscript $z$ represents differentiation with respect to depth. The offshore coordinate is $x$.

Figure 14 shows regularly gridded sections of the alongshelf geostrophic velocity, computed for winter (February-March) and summer (August-September) using the thermal wind relation. Barotropic currents derived from mean near-bottom current meter observations (taken from *Beardsley et al.*, [1985]) have been added to provide a nonzero velocity at the bottom; the bottom values are taken from Figure 5. The geostrophic velocity calculations indicate a mean westward shelf flow of greater than 0.05 m $s^{-1}$ to the west during both seasons. Flow over the shelf is predominantly barotropic, since horizontal density gradients are weak on the shelf throughout the year. The dominant feature is the baroclinic frontal jet. The jet width is 15 km at the surface, with a core velocity in excess of 0.15 m $s^{-1}$ during winter and 0.25 m $s^{-1}$ in summer.

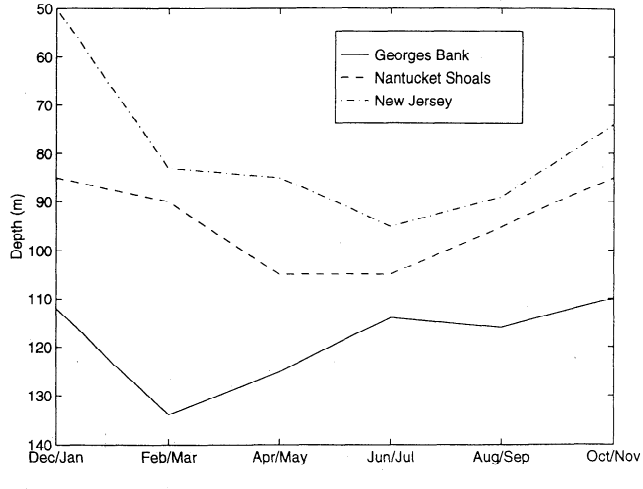


**Figure 13.** The seasonal variations of the bottom outcrop of the front, as determined by the 34.5 isohaline, for the three regions.

The maximum jet velocity in the NS region varies seasonally by a factor of roughly 2, with the strongest velocities in the spring and the weakest in the winter (temporarily assuming a level of no motion along the bottom). The strength of the NS surface jet is a minimum, 0.17 m $s^{-1}$, during December-January and a maximum, 0.30 m $s^{-1}$, during April-May. (From Figure 7, the maximum density contrast is during the summer, but this is limited to the lower half of the water column. During spring, the full depth-integrated density contrast is stronger than in summer, even though the horizontal density gradients are larger in summer near the bottom.) The maximum jet velocity ranges between 0.17 and 0.23 m $s^{-1}$ for the other time periods. The annual mean maximum jet velocity is 0.22 m $s^{-1}$ to the west.

The maximum jet velocity is weaker in the GB and NJ regions (see Table 2). The GB maximum jet velocity, averaged over the six time periods, is 0.15 m $s^{-1}$ to the west. During December-January, the jet is at its peak strength of 0.23 m $s^{-1}$. The jet strength reaches a minimum of 0.07 m $s^{-1}$ during August-September. The NJ maximum jet velocity averaged over the six time periods is comparable to GB.

The offshore position of the jet core varies seasonally in all three regions, migrating onshore through the spring and summer with a large offshore translation between late fall and winter. The NS jet core ranges from between 12 km offshore (December-January) to 3 km

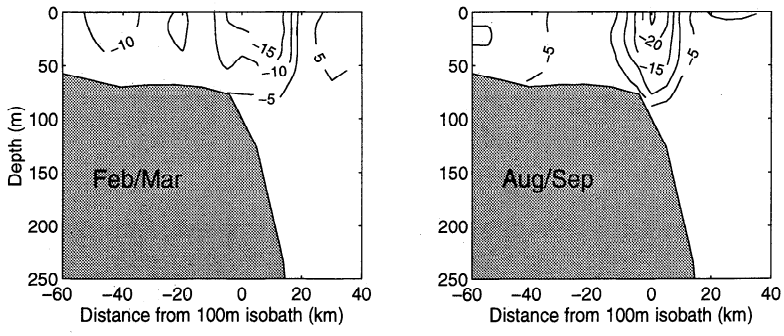


**Figure 14.** Winter and summer geostrophic velocity sections in the NS region. The bottom reference velocities from Figure 5 (the NSFE experiment) have been added. The contour interval is 0.05 m $s^{-1}$.

onshore (October-November) of the 100-m isobath. The annual mean position of the NS jet core is 5 km offshore of the 100-m isobath or above the 125-m isobath. The GB and NJ jet cores have similar seasonal trends. The annual mean location of the GB jet is 14 km offshore of the 100-m isobath or above the 275-m isobath, while the annual mean location of the NJ jet is 7 km offshore of the 100-m isobath or above the 150-m isobath.

We have computed frontal jet widths based on the contour of half of the maximum surface velocity. The results showed very little seasonal variability for any region. The NS jet is approximately 15-20 km wide except for December-January, when it is roughly 40 km wide. The annual mean width of the NS jet is approximately 21 km. The NJ jet is consistently 10-20 km wide, while the GB jet is generally double this width.

The vertical scale of the baroclinic jet, again defined by half the maximum velocity, did not vary seasonally for NS, being roughly 60 m throughout the year. On average, the GB jet extended an extra 15 m deeper than NS, also with little seasonal variation. The average depth of the NJ jet is 55 m, with more substantial seasonal variability. In each region, the baroclinic jets reach their peak depths during December-January, corresponding to the period of weakest horizontal density gradients.

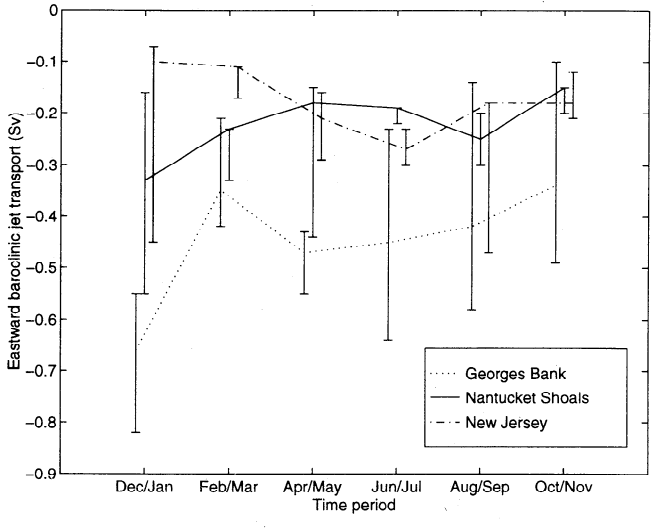


**Figure 15.** Seasonal variations of the baroclinic jet transport (defined by either half of the velocity maximum or 0.05 m $s^{-1}$, whichever is greater), for each of the time periods from the three regions. The bottom velocity is assumed to be zero for all three regions.

The transport within the baroclinic jet has been calculated, defining the horizontal extents by the points at which the surface velocity decreases to 0.05 m $s^{-1}$ to the west. This corresponds to roughly 15 km across-shelf for NS. Should this criteria not be satisfied, a maximum extent of 30 km in either direction from the core of the surface jet is used. Once the horizontal scale has been established, the transport is integrated over the entire water column between these two points. The results are shown in Figure 15 . For NS, the jet transport remained between 0.20 and 0.32 Sv to the west. The NS annual mean jet transport is 0.24 plus or minus 0.12 Sv. (Errors are estimated using one standard deviation of temperature and its effect on the density field from Figure 10 and then using the revised density field to compute a new baroclinic jet transport.) Transport within the NJ jet was slightly smaller in magnitude (annual mean of 0.16 plus or minus 0.16 Sv). The GB jet transport is about twice the NS transport due primarily to the larger jet size and peaks in December-January at 0.65 Sv. The rest of the year it remained fairly constant at 0.42 Sv to the west, however, giving an annual mean westward transport of 0.45 plus or minus 0.17 Sv. It is likely that this decrease in transport to the southwest implies a loss of shelf or frontal water to the continental slope region, but this cannot be ascertained from the climatology. This would be consistent with the results of *Biscaye et al.* [1994] from SEEP II, who found that the shelf transport in the southern portion of the Middle Atlantic Bight was only 0.19 Sv. This implies that the shelf transport had been reduced by half from Nantucket Shoals down to the Chesapeake Bay region.

## 6. Potential Vorticity Structure

With the fields of stratification and geostrophic velocity, we can now compute the inviscid potential vorticity distribution within the frontal region. This is defined

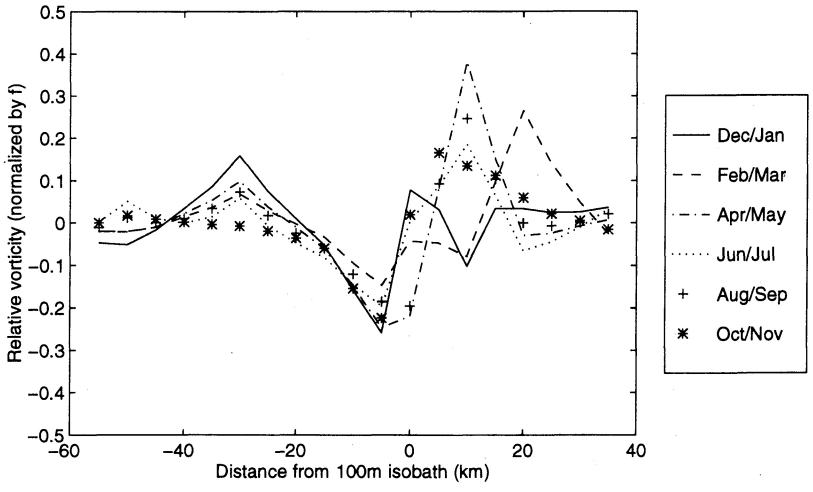


**Figure 16.** The cross-shelf variation of the relative vorticity in the 5- to 25-m depth range for each time period in the NS region. The relative vorticity is scaled by the Coriolis parameter, $f$=1 × $10^{-4}$ $s^{-1}$.

as

$$q = \frac{-1}{\rho_0}[(f - \frac{\partial v}{\partial x})\frac{\partial \rho}{\partial z} + \frac{\partial v}{\partial z}\frac{\partial \rho}{\partial x}] \quad (2)$$

where $q$ is the potential vorticity in units of $m^{-1}$ $s^{-1}$, $\rho_0$ is the mean density, $f$ is the Coriolis parameter, and $x$ and $z$ are the offshore and vertical coordinates. The potential vorticity is obtained by finite differencing the density and velocity fields. Similarly, the relative vorticity,

$$\zeta = \frac{\partial v}{\partial x} \quad (3)$$

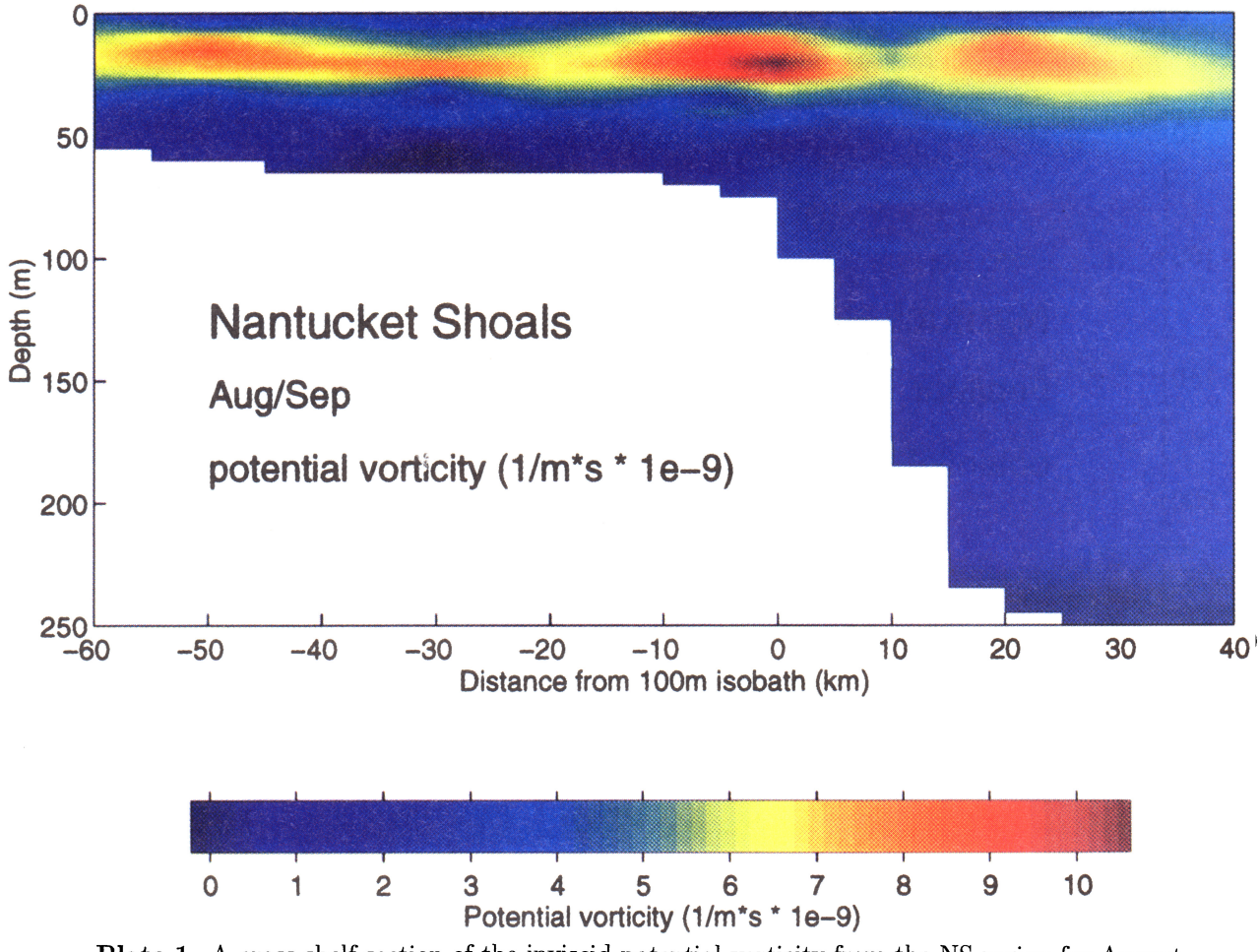


**Plate 1.** A cross shelf section of the inviscid potential vorticity from the NS region for August-September. The colorbar indicates the value of the potential vorticity.

is obtained from the geostrophic velocity field using a finite difference method.

The dominant feature in the relative vorticity is the baroclinic jet. Because of the velocity maximum just seaward of the shelfbreak, there is a region of cyclonic shear seaward of the jet core, as the along-shelf decreases offshore, and a region of anticyclonic shear shoreward of the jet core. This is evident in Figure 16, which shows the relative vorticity averaged between depths of 5 and 25 m for each of the bimonthly time periods. The maximum cyclonic shear occurs during the April-May time period, when the jet velocity is a maximum, and reaches a value of $\zeta/f$=0.4. During the other time periods, the maximum cyclonic shear ranges from 0.2 to 0.4. On the shoreward side of the jet, the magnitude of the anticyclonic shear is roughly half this value, ranging from $\zeta/f$=-0.1 to -0.2. These relative vorticities are about half of those measured by *Gawarkiewicz et al.* [1996] in July in the NJ region. (The NJ value of $\zeta/f$ for June-July is 0.15.)

The potential vorticity during the summer is dominated by the seasonal stratification. Plate 1 shows the potential vorticity from the August-September time period in the Nantucket Shoals region. The maximum values of 7-10 $m^{-1}$ $s^{-1}$ are in the seasonal pycnocline, between depths of 10 and 30 m.

During the winter (Plate 2), the largest value of the potential vorticity is near the foot of the front, with a value of 3 $\times$ $10^{-9}$ $m^{-1}$ $s^{-1}$. This is more than triple the value of the ambient value over the shelf in winter. The potential vorticity maximum slopes upward and offshore along the frontal boundary over the upper slope. During the summer, this local maximum is still present but has a value that is more typically 2 $\times$ $10^{-9}$ $m^{-1}$ $s^{-1}$. The potential vorticity values near the bottom must, of course, be viewed skeptically because frictional effects are likely to affect the local dynamics.

These results show that the cycle of seasonal heating and cooling largely dominates the potential vorticity structure, with contributions from the relative vorticity of the baroclinic jet near the shelfbreak. The asymmetry between the cyclonic and anticyclonic shear is consistent with that of open ocean fronts [e.g., *Bleck et al.*, 1988], where cross-frontal (in this case offshore) flows of buoyant fluid are balanced by return flows of more dense fluid at depth through vigorous vertical circulations. However, the shelfbreak front is quite different from these open-ocean fronts because the frontal isopy-

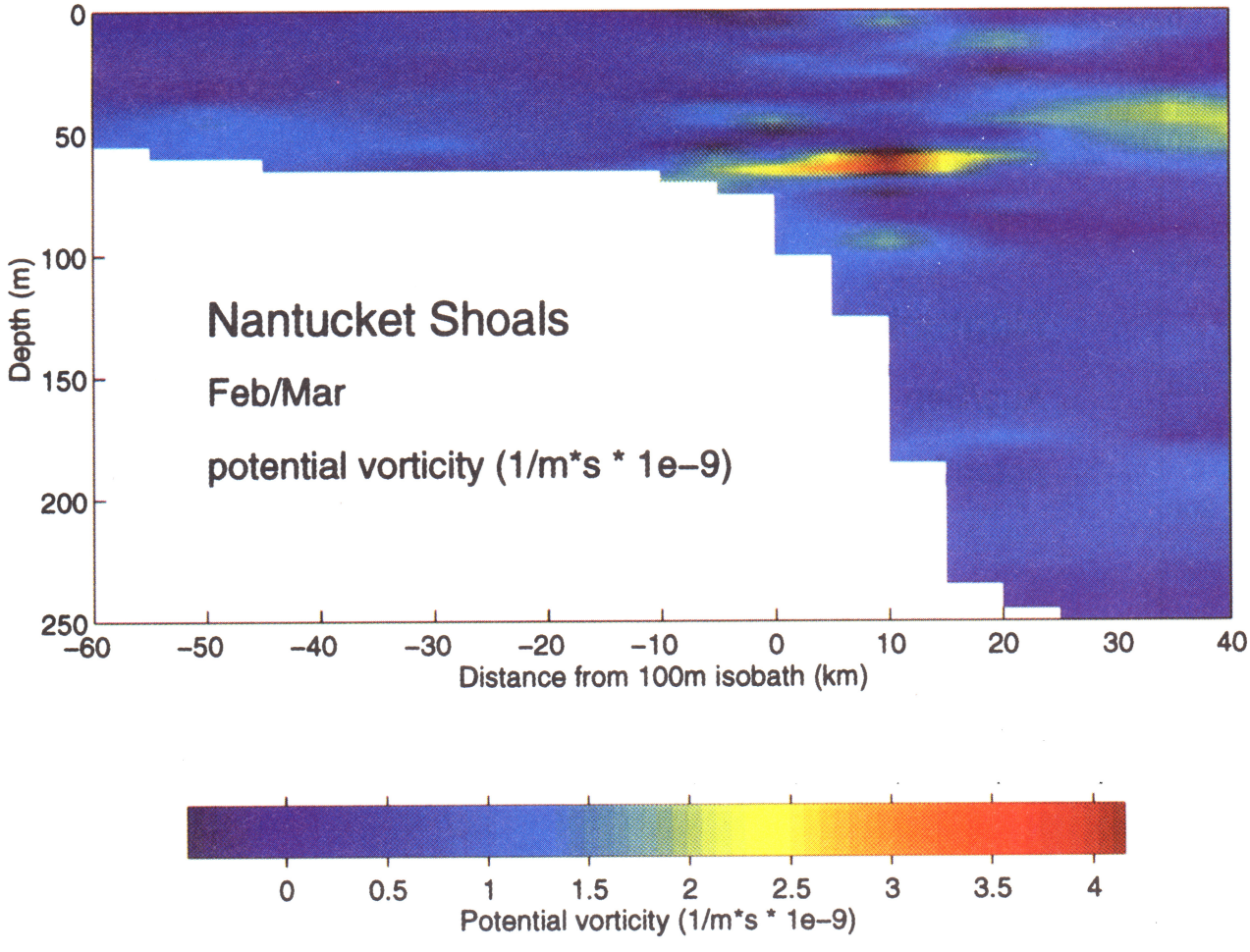


**Plate 2.** A cross-shelf section of the inviscid potential vorticity from the NS region for February-March. Note that the colorbar differs from Plate 1.

cnals intersect the bottom, and thus both bottom topography and bottom boundary layer transports must affect the frontal structure.

## 7. Discussion

This climatology has synthesized over 90 years of hydrographic measurements in the Middle Atlantic Bight using a depth bin averaging method. The products of this climatology have shown close agreement with previously published climatologies, modeling efforts, and synoptic observations. However, this climatology suffers from several limitations. First, an assumption inherent to any seasonal climatology is that interannual variability is minimal compared with the seasonal cycle. Although the temperature follows a well-regulated seasonal cycle, *Manning* [1991] showed that for the MAB salinity, large interannual fluctuations are superimposed on the seasonal cycle. He attributed 70% of this interannual variation to local river runoff and precipitation. Second, slope water averaging results should be interpreted with caution. The continental slope region experiences large temperature and salinity fluctuations associated with the interaction of slope water, warm core rings, and the Gulf Stream. Ideally, further attention should be placed on the cross-isobath gradients within the continental slope region. However, the limited amount of data points, accentuated beyond the 500-m isobath, prohibits a study of this nature at this time. Third, this study was limited by assuming a two-dimensional cross-shelf section in each region. *Chapman and Beardsley's* [1989] oxygen isotope and salinity analysis has shown how the mean flow through the MAB is part of a large-scale coastal current system. Ideally, a three-dimensional climatology, such as that provided by *Naimie et al.* [1994] for the Gulf of Maine, would be useful in also establishing the along-isobath gradients. However, the limited number of stations again is a severe constraint.

Despite its limitations, the climatology is useful in defining the characteristic velocity and length scales associated with the frontal jet and defining the transport associated with the jet. The shelf transport (defined from the 40-m isobath to the onshore edge of the jet) and jet transport (defined previously) have been calculated for the February-March and August-September NS cases, with the NSFE [*Beardsley et al.*, 1983] bottom values included (see Figure 5). The shelf transport is westward, with a value of 0.29 Sv for February-March and 0.18 Sv for August-September. *Beardsley et al.* [1985] observed a higher annual mean shelf transport of 0.383 Sv, which included the shelf transport as well as the frontal jet. The associated westward jet transports were 0.30 Sv (February-March) and 0.28 Sv (August-September). These values are about half of those estimated from two synoptic sections by *Voorhis et al.* [1976] in this region, but are more nearly comparable with *Gawarkiewicz et al.* [1996], who computed a jet transport of 0.38 Sv from their synoptic acoustic doppler current profiler (ADCP) section. (The latter however, was in the NJ region). The total shelf and jet transports are 0.59 Sv (February-March) and 0.46 Sv (August-September). Thus the jet comprises 51% of the total (shelf plus jet) transport for February-March and 61% for August-September, based on these estimates. It is clear that the transport within the jet is of roughly the same order as the transport over the entire shelf.

While the climatology cannot be used to estimate transport losses from the shelf and jet onto the slope, we reiterate that the decreasing transport from the GB to NS to NJ regions is consistent with the estimate of *Biscaye et al.* [1994] that half of the shelf transport is lost offshore between Nantucket Shoals and the vicinity of Chesapeake Bay in the southern portion of the Middle Atlantic Bight. This ratio is similar to the decreasing jet transport from NS or GB to NJ. Further work is necessary to relate shelf and jet transport along the Middle Atlantic Bight to shelf losses to the continental slope region.

The jet transport has important implications when considering processes by which shelf water is carried out onto the slope, in particular on streamers of shelf water ejected onto the slope by warm core rings [e.g., *Bisagni*, 1983; *Joyce et al.*, 1992]. The transport estimate by *Joyce et al.* [1992] for the offshore transport of shelf water onto the slope in a streamer was 0.4 Sv, which is comparable to the entire shelf transport between the 40- and 100-m isobaths measured by *Beardsley et al.* [1985]. More recently, R. J. Schlitz (The interaction of shelf water with warm-core rings, submitted to *Journal of Geophysical Research*, 1997) has shown a range of streamer transports varying from 0.5 Sv in the direction of the ring to 0.35 Sv in the direction opposite to the ring. It is a distinct possibility that the large transports within the streamers result from an offshore diversion of the frontal jet, as forced by the proximity of a warm-core ring. Further work is necessary to clarify this issue; however, Schlitz has shown that much of the water within the streamers appears from the frontal region, which is consistent with this speculation.

The cross-frontal distribution of potential vorticity in the surface layer shows quite clearly that there is a local maximum associated with the surface expression of the jet. Near the maximum, the sign of the potential vorticity gradient reverses, which is a necessary condition for instability. Thus the climatological mean frontal state allows for the possibility of instabilities.

Finally, it is interesting to note that the strongest cross-shelf density gradients occur near the foot of the front. This leads to large vertical velocity shear near the foot of the front and, in the NS region, a jet which is located relatively close to the shelfbreak, as opposed to the location of the surface outcrop of the front. This is interesting in that it confirms the dynamical importance of the foot of the front, as *Gawarkiewicz and Chap-*

*man* [1992] suggested in an idealized numerical modelling study. Subsequent work by *Chapman and Lentz* [1994, 1997] has shown how thermal wind shear within the bottom boundary layer may act to inhibit the offshore flow of water carried within the bottom boundary layer. This climatology strongly suggests that the cross-frontal density gradients near the foot of the front are strong enough to allow the thermal wind shear to affect the offshore transport within the bottom boundary layer.

## 8. Conclusions

Using historical hydrographical data which we have collapsed onto two-dimensional cross-shelf sections, we have investigated the seasonal evolution of the shelfbreak front and its associated frontal jet. Typical velocity scales which emerge from this study are 0.2-0.3 m $s^{-1}$ maximum jet velocities and widths of roughly 20 km. Comparison with previously reported synoptic sections gives climatological velocity scales and widths which are roughly half as large in velocity and about double the width relative to synoptic sections. Relative vorticities are greater on the seaward, cyclonic side of the jet, ranging from 0.2 to 0.4 $f$. The relative vorticity on the shoreward side of the jet is roughly half this value.

Much of the vertical velocity shear in the core of the jet is concentrated near the foot of the front, where the cross-shelf density gradients are the greatest. In the Nantucket Shoals region, the mean annual position of the core of the jet is 5 km seaward of the 100-m isobath, with a seasonal drift of 15 km. Much more work is necessary to clarify the structure and dynamics of the front.

**Acknowledgments.** C. L. was supported by the Naval Oceanographic Command and Naval Post-Graduate School. G. G. appreciates the support of the Office of Naval Research, Physical Oceanography Program, under grant N00014-95-1-0575, as well as the support of the GLOBEC program under grant OCE-9529402. Thanks to Veta M. Green for ably preparing the manuscript. The authors appreciate the efforts of J. Lynch of WHOI, who coadvised C. L. during his stay in the Joint Program, A. Newhall for programing help, and R. Curry for introducing us to HydroBase and answering many questions. We also thank D. Chapman for comments on an early version of the manuscript and S. Lentz for helpful comments during the course of the work.

## References

Aikman, F., III, Pycnocline development and its consequences in the Middle Atlantic Bight, *J. Geophys. Res., 89*, 685-694, 1984.

Aikman, F., III, H. W. Ou, and R. W. Houghton, Current variability across the New England continental shelf-break and slope, *Cont. Shelf Res., 8*, 625-651, 1988.

Beardsley, R. C., and C. N. Flagg, The water structure, mean currents, and shelf/slope water front on the New England continental shelf, *Mem Soc. R. Sci. Liege, 6*(X), 209-225, 1976.

Beardsley, R. C., C. A. Mills, J. A. Jermersch Jr., W. S. Brown, N. Pettigrew, J. Irish, S. Ramp, R. Schlitz, and B. Butman, Nantucket Shoals Flux Experiment (NSFE79), 2, Moored array data report, *Tech. Rep. WHOI-83-13*, 140 pp., Woods Hole Oceanogr. Inst., Woods Hole, Mass., 1983.

Beardsley, R. C., D. C. Chapman, K. H. Brink, S. R. Ramp, and R. Schlitz, The Nantucket Shoals Flux Experiment (NSFE79), I, A basic description of the current and temperature variability, *J. Phys. Oceanogr., 15*, 713-748, 1985.

Bigelow, H. B., Studies of the waters on the continental shelf: Cape Cod to Chesapeake Bay, I, The cycle of temperature, *Pap. Phys. Oceanogr. Meteorol., 2*, 1-135, 1933.

Bisagni, J. J., Lagrangian current measurements within the eastern margin of a warm-core Gulf Stream ring, *J. Phys. Oceanogr., 13*, 709-715, 1983.

Biscaye, P. E., C. N. Flagg, and P. G. Falkowski, The Shelf Edge Exchange Processes Experiment, SEEP-II: An introduction to hypotheses, results, and conclusions, *Deep Sea Res., Part II, 41*, 231-252, 1994.

Bleck, R., R. Onken, and J. D. Woods, A two-dimensional model of mesoscale frontogenesis in the ocean, *Q. J. R. Meteorol. Soc., 114*, 347-371, 1988.

Bue, C. D., Stream flow from the United States into the Atlantic Ocean during 1931-60, *U.S. Geol. Surv. Water Supply Pap. 1899-1*, 36 pp., 1970.

Burrage, D. M., and R. W. Garvine, Summertime hydrography at the shelfbreak front in the Middle Atlantic Bight, *J. Phys. Oceanogr., 18*, 1309-1319, 1988.

Chapman, D. C., A simple model of the formation and maintenance of the shelf/slope front in the Middle Atlantic Bight, *J. Phys. Oceanogr., 16*, 1273–1279, 1986.

Chapman, D. C., and R. C. Beardsley, On the origin of shelf water in the Middle Atlantic Bight, *J. Phys. Oceanogr., 19*, 384-391, 1989.

Chapman, D. C., and S. J. Lentz, Trapping of a coastal density front by the bottom boundary layer, *J. Phys. Oceanogr., 24*, 1464-1479, 1994.

Chapman, D. C., and S. J. Lentz, Adjustment of stratified flow over a sloping bottom, *J. Phys. Oceanogr., 27*, 340-356, 1997.

Chapman, D. C., J. A. Barth, R. C. Beardsley, and R. G. Fairbanks, On the continuity of the mean flow between the Scotian Shelf and the Middle Atlantic Bight, *J. Phys. Oceanogr., 16*, 758-772, 1986.

Condie, S. A., Formation and stability of shelf break fronts, *J. Geophys. Res., 98*, 12,405-12,416, 1993.

Curry, R. G., Hydrobase: A database of hydrographic stations and tools for climatological analysis, *Tech. Rep. WHOI-96-01*, 50 pp., Woods Hole Oceanogr. Inst., Woods Hole, Mass., 1996.

Drinkwater, K. F., R. A. Meyers, R. G. Pettipas, and T. L. Wright, Climatic data for the northwest Atlantic: The position of the shelf/slope front and the northern boundary of the Gulf Stream between 50 W and 75 W, 1973-1992, *Can. Data Rep. Fish. and Ocean Sci. 125*, 103 pp., 1994.

Flagg, C. N., B. A. Magnell, D. Frye, J. J. Cura, S. E. McDowell, and R. I. Scarlet, Interpretation of the physical oceanography of Georges Bank, final report, vol. I. prepared for the N. Y. OCS Off., Bur. of Land Manage., by E. G. and G. Environ. Consult., Waltham, Mass., 1982.

Flagg, C. N., R. W. Houghton, and L. J. Pietrafesa, Summertime thermocline salinity maximum intrusions in the

Mid-Atlantic Bight, *Deep Sea Res., Part II, 41*, 325-340, 1994.

Fofonoff, P., and R. C. Millard Jr., Algorithms for computation of fundamental properties of seawater, *UNESCO Tech. Pap. Mar. Sci., 44*, 53 pp., 1983.

Garvine, R. W., K.-C. Wong, and G. Gawarkiewicz, Quantitative properties of shelfbreak eddies., *J. Geophys. Res., 94*, 14,475-14,483, 1989.

Gawarkiewicz, G., Linear stability models of shelfbreak fronts, *J. Phys. Oceanogr., 21*, 471-488, 1991.

Gawarkiewicz, G. G., and D. C. Chapman, The role of stratification in the formation and maintenance of shelf-break fronts, *J. Phys. Oceanogr., 22*, 753-772, 1992.

Gawarkiewicz, G. G., T. G. Ferdelman, T. M. Church, and G. W. Luther III, Shelfbreak frontal structure on the continental shelf north of Cape Hatteras, *Cont. Shelf Res., 16*, 1751-1773, 1996.

Halliwell, G., and C. Mooers, The space-time structure and variability of the shelf water slope and Gulf Stream surface temperature fronts and associated warm-core eddies, *J. Geophys. Research, 84*, 7707-7725, 1979.

Houghton, R. W., F. Aikman III, and H. W. Ou, Shelf-slope frontal structure and cross-shelf exchange at the New England shelf-break, *Cont. Shelf Res., 8*, 687-710, 1988.

Houghton, R. W., C. N. Flagg, and L. J. Pietrafesa, Shelf-slope water frontal structure, motion, and eddy heat flux in the southern Middle Atlantic Bight, *Deep Sea Res., Part II, 41*, 273-306, 1994.

Houghton, R. W., R. Schlitz, R. C. Beardsley, B. Butman, and J. L. Chamberlin, The Middle Atlantic Bight cold pool: Evolution of the temperature structure during summer 1979, *J. Phys. Oceanogr., 12*, 1019-1029, 1982.

Joyce, T. M., J. K. B. Bishop, and O. B. Brown, Observations of offshore shelf-water transport induced by a warm-core ring, *Deep Sea Res., 39*, S97-S113, 1992.

Lozier, M. S., M. McCartney, and W. B. Owens, Anomalous anomalies in averaged hydrographic data, *J. Phys. Oceanogr., 24*, 2624-2638, 1994.

Manning, J., Middle Atlantic Bight salinity: Interannual variability, *Cont. Shelf Res., 11*, 123-137, 1991.

Marra, J., R. W. Houghton, and C. Garside, Phytoplankton growth at the shelf-break front in the Middle Atlantic Bight, *J. Mar. Res., 48*, 851-868, 1990.

Mountain, D. G., The volume of shelf water in the Middle Atlantic Bight: seasonal and inter-annual variability, 1977-1987, *Cont. Shelf Res., 11*, 251-267, 1991.

Naimie, C. E., J. W. Loder, and D. R. Lynch, Seasonal variation of the three-dimensional residual circulation on Georges Bank, *J. Geophys. Res., 99*, 15,967-15,990, 1994.

Pickart, R. S., Space-time variability of the deep western boundary current oxygen core, *J. Phys. Oceanogr., 22*, 1047-1061, 1992.

Voorhis, A. D., D. C. Webb, and R. C. Millard, Current structure and mixing in the shelf/slope water front south of New England, *J. Geophys. Res., 81*, 3695-3708, 1976.

Wang, D.-P., Mutual intrusion of a gravity current and density front formation, *J. of Phys. Oceanogr., 14*, 1191-1199, 1984.

Wright, W. R., The limits of shelf water south of Cape Cod, 1941 to 1972, *J. Mar. Res., 34*, 1-14, 1976.

Wright, W. R., and C. E. Parker, A volumetric temperature/salinity census for the Middle Atlantic Bight, *Limnol. Oceanogr., 21*, 563-571, 1976.

G. Gawarkiewicz, Woods Hole Oceanographic Institution, MS#21, 360 Woods Hole Road, Woods Hole, MA 02543-1541. (e-mail: glen@paddle.whoi.edu)

C. Linder, Massachusetts Institute of Technology/Woods Hole Oceanographic Institution Joint Program in Oceanographic Engineering, Woods Hole, MA 02543. (e-mail: clinder@alum.mit.edu.)

(Received January 15, 1997; revised September 12, 1997; accepted January 14, 1998.)